

POSSIBLE DISINTEGRATING SHORT-PERIOD SUPER-MERCURY ORBITING KIC 12557548

S. RAPPAPORT¹, A. LEVINE², E. CHIANG^{3,4}, I. EL MELLAH^{1,5}, J. JENKINS⁶, B. KALOMENI^{2,7}, E. S. KITE^{4,8}, M. KOTSON¹, L. NELSON⁹, L. ROUSSEAU-NEPTON¹⁰, AND K. TRAN¹

Draft version October 29, 2018

ABSTRACT

We report here on the discovery of stellar occultations, observed with *Kepler*, that recur periodically at 15.685 hour intervals, but which vary in depth from a maximum of 1.3% to a minimum that can be less than 0.2%. The star that is apparently being occulted is KIC 12557548, a $V = 16$ magnitude K dwarf with $T_{\text{eff},s} \simeq 4400$ K. The out-of-occultation behavior shows no evidence for ellipsoidal light variations, indicating that the mass of the orbiting object is less than $\sim 3 M_J$ (for an orbital period of 15.7 hr). Because the eclipse depths are highly variable, they cannot be due solely to transits of a single planet with a fixed size. We discuss but dismiss a scenario involving a binary giant planet whose mutual orbit plane precesses, bringing one of the planets into and out of a grazing transit. This scenario seems ruled out by the dynamical instability that would result from such a configuration. We also briefly consider an eclipsing binary, possibly containing an accretion disk, that either orbits KIC 12557548 in a hierarchical triple configuration or is nearby on the sky, but we find such a scenario inadequate to reproduce the observations. The much more likely explanation—but one which still requires more quantitative development—involves macroscopic particles escaping the atmosphere of a slowly disintegrating planet not much larger than Mercury in size. The particles could take the form of micron-sized pyroxene or aluminum oxide dust grains. The planetary surface is hot enough to sublimate and create a high-Z atmosphere; this atmosphere may be loaded with dust via cloud condensation or explosive volcanism. Atmospheric gas escapes the planet via a Parker-type thermal wind, dragging dust grains with it. We infer a mass loss rate from the observations of order $1 M_{\oplus}/\text{Gyr}$, with a dust-to-gas ratio possibly of order unity. For our fiducial $0.1 M_{\oplus}$ planet (twice the mass of Mercury), the evaporation timescale may be ~ 0.2 Gyr. Smaller mass planets are disfavored because they evaporate still more quickly, as are larger mass planets because they have surface gravities too strong to sustain outflows with the requisite mass-loss rates. The occultation profile evinces an ingress-egress asymmetry that could reflect a comet-like dust tail trailing the planet; we present simulations of such a tail.

Subject headings: eclipses — occultations — planets and satellites: general — stars: planetary systems

1. INTRODUCTION

The *Kepler* mission has now discovered some ~ 1250 very good exoplanet candidates via planetary transits of the parent star (Borucki et al. 2011). The transit depths range from a few percent for giant gas planets to $\lesssim 10^{-4}$ for smaller planets that are of the size of the Earth. The

distribution of orbital periods for these systems is shown in Fig. 1. The bulk of the systems have periods between ~ 3 and 30 days. As observations continue to be accumulated and analyzed, the newly discovered candidates will tend to be longer period systems; the short-period end of the period distribution will change relatively slowly. There are relatively few systems with periods below a few days, and furthermore, most of the systems shown in Fig. 1 with orbital periods less than a day are either now considered to be false positives (i.e., they are most likely associated with background blended binaries) or have not yet been followed up in the detail required for conclusive categorization (Borucki et al. 2011). The confirmed short-period planets, most of which were not discovered by *Kepler*,¹¹ have orbital periods between 0.73 and 1.09 days. These orbital periods are indicated by dual arrows in Fig. 1.

The shortest planetary orbital period that has been reported is 17.8 hours (Winn et al. 2011).¹² The planet 55 Cnc e, the innermost of 5 planets revolving around 55 Cnc, was discovered with ground-based optical Doppler

¹ 37-602B, M.I.T. Department of Physics and Kavli Institute for Astrophysics and Space Research, 70 Vassar St., Cambridge, MA, 02139; sar@mit.edu

² 37-575, M.I.T. Kavli Institute for Astrophysics and Space Research, 70 Vassar St., Cambridge, MA, 02139; aml@space.mit.edu

³ Department of Astronomy, UC Berkeley, Hearst Field Annex B-20, Berkeley CA 94720-3411; echiang@astro.berkeley.edu

⁴ Department of Earth and Planetary Science, UC Berkeley, 307 McCone Hall, Berkeley CA 94720-4767

⁵ ENS Cachan, 61 avenue du Président Wilson, 94235 Cachan, France; ielmellah@ens-cachan.fr

⁶ SETI Institute/NASA Ames Research Center, Moffett Field, CA 94035; Jon.M.Jenkins@nasa.gov

⁷ Department of Astronomy and Space Sciences, University of Ege, 35100 Bornova-Izmir, Turkey; Department of Physics, Izmir Institute of Technology, Turkey

⁸ Division of Geological and Planetary Sciences, Caltech MC 150-21, Pasadena CA 91125; ekite@caltech.edu

⁹ Department of Physics, Bishop's University, 2600 College St., Sherbrooke, QC J1M 1Z7; lnelson@ubishops.ca

¹⁰ Département de physique, de génie physique et d'optique Université Laval, Québec, QC G1K 7P4; laurie.nepton.1@ulaval.ca

¹¹ Taken from the “Exoplanet Orbit Database” at <http://exoplanets.org>, produced by Jason Wright, Geoff Marcy, and the California Planet Survey consortium.

¹² Only just recently an exoplanet with an even shorter orbital period, KOI 961.02, with $P_{\text{orb}} = 10.9$ hours, was reported (Muirhead et al. 2012).

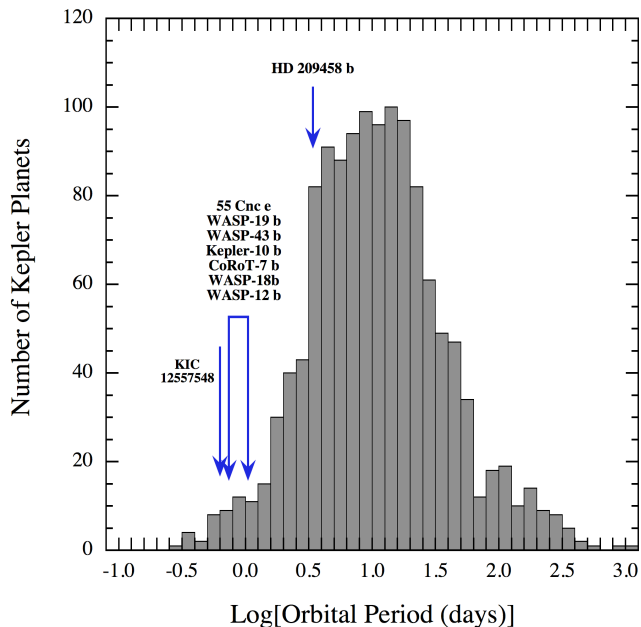


Figure 1. Distribution of orbital periods among the exoplanet candidates discovered with *Kepler*. The shorter period planets specifically named are not necessarily from the *Kepler* survey and are taken from the on-line catalog “The Exoplanet Orbit Database” (see text).

measurements (Fischer et al. 2008; Dawson & Fabrycky 2010) and detected in transit by extensive satellite observations with the *MOST* satellite (Winn et al. 2011). Winn et al. (2011) estimate its mass and radius to be $\sim 9 M_{\oplus}$ and $2 R_{\oplus}$. Planet orbits considerably shorter than a day are, in principle, quite possible, and their detection via transits using *Kepler* should not be problematic in a signal-to-noise sense. There are at least two reasons, however, why such close-in, short-period planets have not been heretofore emphasized. First, there are many short-period stellar binaries that, when their light is highly diluted by another star within a few arc seconds (e.g., the target star under observation by *Kepler*), are hard to distinguish from stars with transiting planets. Second, giant planets are expected to be destroyed by Roche lobe overflow if they are heated too strongly by their parent stars (Batygin, Stevenson, & Bodenheimer 2011).

With *Kepler* data, the orbital period P_{orb} of a planet about a star can be measured. If the orbit is circular, and the planet has a mass M_p much less than the mass of the parent star, then the size of its Roche lobe can be determined without knowing the mass of the parent star:

$$R_L \simeq 1.95 \left(\frac{M_p}{M_J} \right)^{1/3} \left(\frac{P_{\text{orb}}}{\text{days}} \right)^{2/3} R_J \quad (1)$$

where M_J and R_J are the mass and radius of Jupiter, respectively. Therefore, even if the planet does not evaporate because of the strong stellar radiation field, by the time a Jupiter-mass planet migrates to an orbit with $P_{\text{orb}} \lesssim 9$ hours, it will start to empty its envelope via Roche-lobe overflow.

In this work we discuss the signature of a planet in a 15.685-hour orbit about a K star. The object came to

our attention via periodic occultations of the target star KIC 12557548. The term “occultation” is perhaps more appropriate than “transit” (although we will use both terms interchangeably in this paper), because of the fact that the depths of the events are highly time dependent. As we discuss in this work, the occultations are periodic to 1 part in 10^5 or more, and therefore must be due to the presence of an orbiting companion. However, the variation of the eclipse depths rules out transits by a single opaque body. More likely, we argue, the occultations are due to a stream of dust particles resulting from the slow disintegration of the planet.

In §2.2–2.5 of this work we describe detailed analyses of the *Kepler* observations of KIC 12557548 from quarters Q2 through Q6. In these sections we present light curves as well as power density spectra of the light curves. We also present an optical spectrum which basically confirms the spectral properties of KIC 12557548 given in the Kepler Input Catalog (KIC). In §3 we outline three explanations for the variable occultation depths, including grazing transits due to a pair of planets; an eclipsing binary, possibly containing an accretion disk, that orbits KIC 12557548 in a hierarchical triple configuration; or, more likely, obscuration by a stream of debris from a disintegrating planet. We explore in §4 the hypothesis of an occulting dust cloud in some depth. In particular, we discuss how dust can be stripped off a planet with substantial gravity. We go on to compute the approximate shape of a dust stream that has left the planet and is shaped by radiation pressure. Our findings are summarized in §5; there we also suggest future observations that may robustly establish the nature of the variable occultation depths.

2. DATA ANALYSIS

2.1. Discovery

The occultations of KIC 12557548 were discovered as part of a systematic search through the *Kepler* data base for eclipsing binaries that are not in the Prsa et al. (2011) catalog. We used publicly available quarter 2 (“Q2”) data from each of the $\sim 150,000$ *Kepler* targets to carry out a general Fourier transform search for periodicities (Kotson et al. 2012). The criteria for declaring a particular power density spectrum (PDS) as “interesting” are that (i) there is at least one peak with amplitude greater than 5 standard deviations above the local mean of the spectrum, and (ii) there is at least one harmonic or sub-harmonic of the largest peak that is at least 3 standard deviations above the local mean.

In all, we find that ~ 4800 power spectra contain interesting content, as defined above. Of these, approximately 1800 are binaries that are already in the Prsa et al. (2011) catalog, as well as some 300 binaries, mostly of the contact variety, that appear to have not made it into that catalog (Kotson et al. 2012). Most of the remaining FFTs of interest involve stars that exhibit pulsations of one sort or another.

One of the interesting power spectra contains a peak at 15.6854 hours and 15 harmonics thereof with amplitudes that decrease slowly with frequency. This is indicative of a sharp transit/eclipse/occultation which occupies only a small fraction of a cycle. The target, KIC 12557548, does not appear in either the Prsa et al. (2011) binary

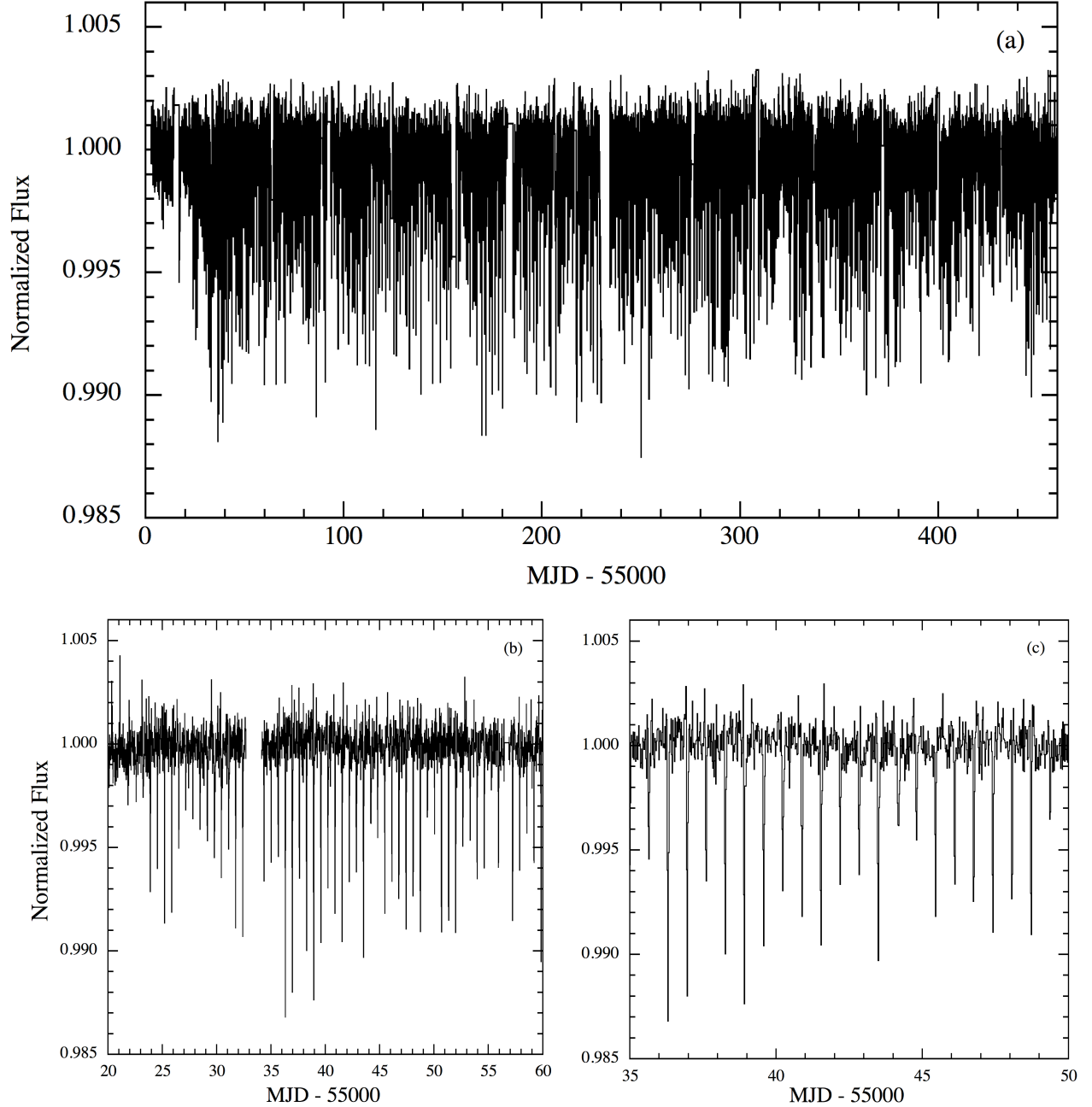


Figure 2. Light curves for KIC 12557548 spanning the Q2–Q6 data sets, as well as for 40-day and 15-day segments of the Q2 data. The intrinsic Poisson fluctuations per ~ 30 -min *Kepler* sample are $\sim 0.03\%$.

star catalog or the Borucki et al. (2011) planet catalog.

2.2. Light Curves

Light curves for KIC 12557548 are shown in Fig. 2. The plots shown in this figure were made by combining the raw (SAP.FLUX) long-cadence light curves from quarters 2 through 6 (Q2–Q6); before this was done the light curves from the various different quarters were multiplied by relative scale factors chosen to minimize any differences in intensity across quarter boundaries. Low frequency variations caused by instrumental, and possibly intrinsic source, variations were then removed by convolving the flux data with a boxcar of duration 0.65356 days (15.5854 hours) and then subtracting the convolved

flux curve from the pre-convolution light curve. This processing should largely preserve the actual source behavior on orbital and suborbital timescales.¹³

Fig. 2 shows the highly variable nature of the occultations which, in fact, have depths that render them easily seen over most of the 460 day interval, but for the first ~ 22 days of Q2 are very small or even not noticeable. We have also checked the Q1 data and, indeed, the occultations are not apparent during the first 10 days as well as the final 10 days of that quarter. As seen in panel (c)

¹³ We also used the PyKE software to process the data. See <http://keplergo.arc.nasa.gov/ContributedSoftwarePyKEP.shtml>

of Fig. 2, the individual occultations vary strongly from one cycle to the next. The variable occultations persist, with a similar range in depths, throughout the following 438 days of Q2 through Q6 data.

When the data are folded about the 15.685-hour period, the results, shown in Fig. 3, further illustrate how the occultation depths vary. The largest depth is $\sim 1.3\%$, while some of the points near the middle of the occultation are depressed by no more than $\sim 0.15\%$. On the other hand, it is clear that, aside from a few individual data points within the occultation interval, almost *all* show a minimum depression in the intensity by $\sim 0.1\%$. Thus, even when the occultations are not noticeable, there still may be a small effect.

When the folded data are binned (see Fig. 3b) one can see that the average depth at the heart of the occultation is only $\sim 0.6\%$ or about half the maximum depth. There is evidence (at the $\sim 5\text{-}\sigma$ level) for a small peak in the flux of amplitude $\sim 3 \times 10^{-4}$ at phases up to $\sim 30^\circ$ before the occultation ingress. There is also a very significant depression or deficit in the expected flux over a similar range of phases just after egress. We will discuss these features briefly in Section §4.7.

The full width of the occultation, with the exception of these small features, is 0.1 of the orbital cycle. This corresponds to ~ 1.5 hours in duration, or just 3 *Kepler* long-cadence integration times. If this duration is interpreted simply as indicating the sum of the radii of the occulting “bodies” it corresponds to $(R_1 + R_2)/a \simeq 0.3$. However, if we take into account approximately the effect of the finite integration time, then $(R_1 + R_2)/a \simeq 0.24$. Note that these estimates assume, without justification, equatorial as opposed to grazing occultations.

We have fitted a constant plus a cosine with a period of 15.685 hr and a cosine of half that period to the folded light curve, excluding points inside the occultation interval (i.e., at orbital phases of ± 0.085 cycles around mid occultation), in order to search for possible ellipsoidal light variations. We find only an upper limit of $\sim 5 \times 10^{-5}$ for the amplitude of such features. This limit will be discussed below in the context of setting a constraint on the mass of any body orbiting the target K star.

Finally, we find the epoch of mid-occultation in order to project ahead to future observations:

$$t_n = 55399.824(2) + n \times 0.65356(1) \text{ MJD}, \quad (2)$$

where the numbers in parentheses are the respective uncertainties in the last significant figure given.

2.3. Fourier Search for Modulations

As a check for periodic modulations of the occultation depths for the 15.685-hour period, we carried out an FFT of the Q2 plus Q3 data but with the portions of the light curve away from the occultation set equal to the mean out-of-occultation intensity. The purpose of this latter step is to suppress the noise level, without sacrificing any significant fraction of the signal. The results are shown in Fig. 4. All 16 harmonics of the 15.865-hour period, out to the Nyquist limit, are clearly visible. In addition, a careful inspection of the amplitudes between the harmonics indicates some evidence for low-amplitude modulation-induced sidebands. However, at least a number of these can be reproduced in an FFT of the window

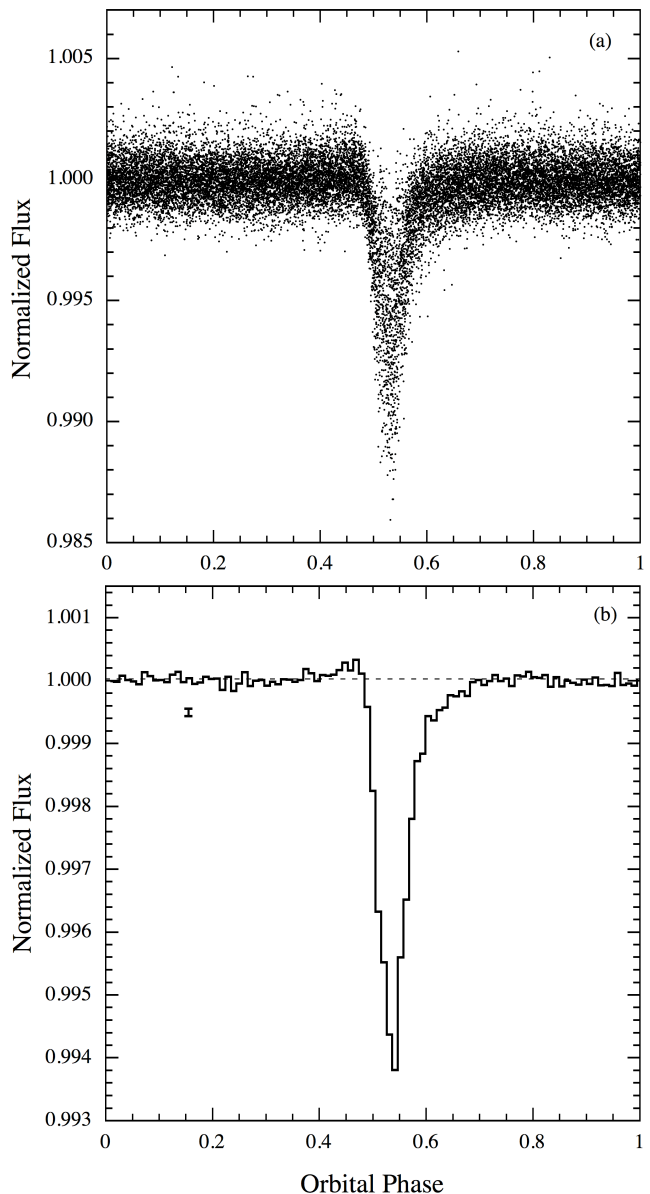


Figure 3. Folded light curves of KIC 12557548 about the 15.685-hour occultation period for the Q2–Q6 data sets. Top panel – unbinned data; bottom panel – folded data averaged into 96 discrete bins (3 bins $\simeq 1$ long-cadence *Kepler* integration time). Short illustrative vertical bar on the left is \pm the standard error of the data points within a bin. Note the highly statistically significant depressed flux level following the main occultation.

function associated with the occultations. Thus, we find no compelling evidence for periodic modulation of the occultation depths.

2.4. Checks on the Validity of the Data

Because of the unusual exoplanet phenomenon presented in this work, we need to be especially careful to ensure that there are no spurious artifacts in the *Kepler* data for this object. In this regard, we performed a number of tests on the data.

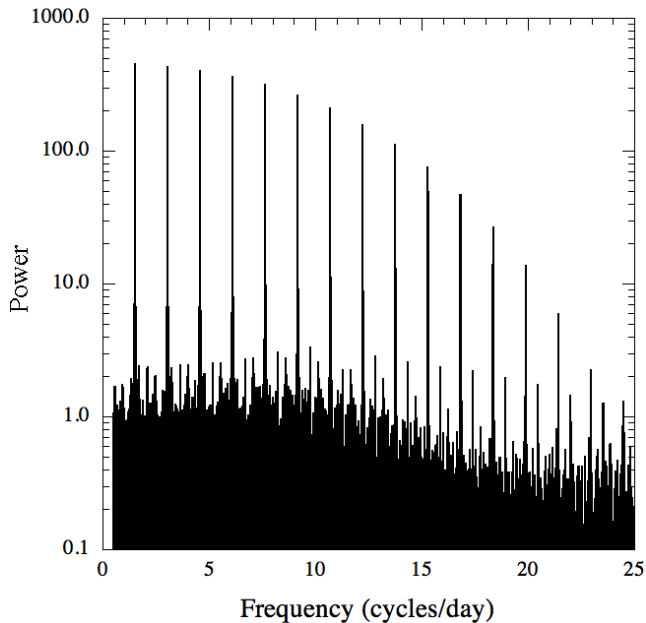


Figure 4. Power spectrum of the detrended flux data for KIC 12557548 with the out-of-occultation region set equal to the mean flux level. See text for details.

First, as mentioned above, we checked that the occultations are present in all of the quarters of released (i.e., public) data (Q1–Q6), and that the behavior of the occultations does not change abruptly across quarterly boundaries.

Second, we investigated whether the photometric variations of KIC 12557548 could be from another star or source on the sky. We examined the Digitized Sky Survey images and found that there are no especially bright stars close to KIC 12557548 whose light or transferred charge might introduce spurious signals into the data stream (i.e., none with $V < 13$ within $3'$ and none with $V \lesssim 10$ within $8'$). An examination of a *Kepler* Full Frame Image for Q1 indicates that there are no obvious stars within $\sim 38''$ (~ 10 pixels). The *Kepler* Input Catalog does list two $Kp=19$ stars located $14''$ and $17''$ from KIC 12557548 (approximately 3.5 and 4.25 pixels), but these could not be the source of the photometric variations for two reasons. (i) We checked difference images for each of Q1–Q6 and the apparent source of the photometric variations is coincident with the stellar image of KIC 12557548 (Batalha et al. 2010). Difference images compare the in-transit frames with out-of-transit frames in the neighborhood of each transit and these are averaged across all events in each quarter. (ii) Analysis of the correlation of the astrometry (brightness weighted centroids) with the photometric signature of the occultations indicates that the position of KIC 12557548 shifts by no more than ~ 0.2 millipixels in either row or column during any quarter. This indicates that there is no other background source that is producing the occultations and that is offset by $\sim 2''$ or more from KIC 12557548, given the depth of the events and the brightness of KIC 12557548 (Jenkins et al. 2010).

As a further check against video crosstalk from the adjacent CCD readout channels, we examined areas on the sky located at the same row/column position on these adjacent channels, and found no stars within $11''$ of the

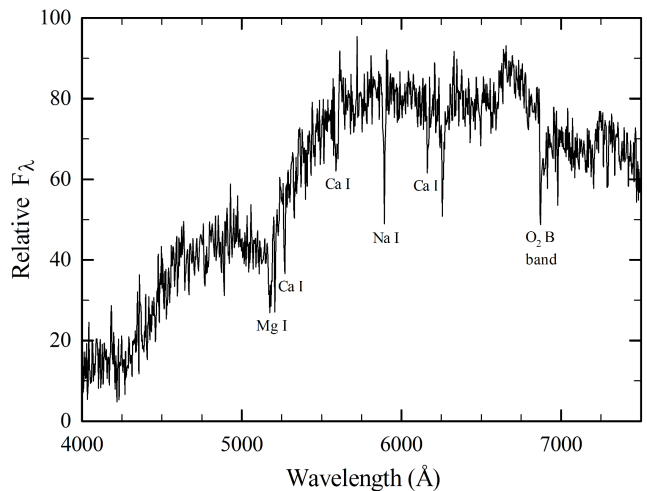


Figure 5. Optical spectrum of KIC 12557548 taken on December 16, 2011 at the OMM Observatory. The spectrum is a stack of four 15-minute exposures through ~ 1.6 air masses. The spectral features are indicative of a mid-KV star.

row/column position of KIC 12557548. The fact that the video crosstalk coefficients vary by typically 50% or more from quarter to quarter as the stars are rotated about the focal plane, and can be either negative or positive, and the fact that the photometric signatures of the occultations are consistent from quarter to quarter, provide additional confidence that it is highly unlikely that the photometric variations are due to a source on an adjacent CCD readout channel.

Third, there are no binaries in the Prsa et al. (2011) catalog or planets in the Borucki et al. (2001) catalog with periods that match that of KIC 12557548.

2.5. Optical Spectrum

KIC 12557548 is a ~ 16 th magnitude star located at $RA(J2000) = 19^h 23^m 51.89^s$ and $Dec(J2000) = 51^\circ 30' 17.0''$. We were able to obtain an optical spectrum of it on 2011 December 16 using the Observatoire Astronomique du Mont-Mégantic’s 1.6-m telescope. Four 15-minute exposures were taken through 1.4 to 1.7 air masses soon after astronomical twilight. The spectrometer utilized the STA0520 blue CCD and a 600-line/mm grating, yielding an effective spectral resolution of 4.3 \AA .

The four spectra were background subtracted, corrected for the quantum efficiency of the detector and the reflectance of the grating, corrected for Rayleigh scattering in the atmosphere, and co-added to produce the spectrum shown in Fig. 5. We did not carry out absolute flux calibrations since the purpose of this observation was simply to confirm the spectral class of the *Kepler* target and to check for any unexpected spectral features.

Despite the relatively low signal to noise ratio of this spectrum, taken under non-ideal conditions, we can clearly see the signatures of a mid-K star. Comparisons with standard stars (see, e.g., Jacoby, Hunter, & Christian 1984) indicate a spectral type of $\sim K4V$. Furthermore, we find that the equivalent width of the Na I line is $3.6 \pm 0.4 \text{ \AA}^{14}$ which is indicative of a K5–K7 star (Jaschek

¹⁴ This is actually an upper limit to the EW because the ISM is

& Jaschek 1987). From this range of spectral types we infer $T_{\text{eff},s} \simeq 4300 \pm 250$ K, a mass of $M_s \simeq 0.70^{+0.08}_{-0.04} M_\odot$, and a radius of $R_s \simeq 0.65^{+0.05}_{-0.04} R_\odot$, assuming that the star is close to the ZAMS. These are all quite consistent with the values listed in the KIC.

The KIC lists magnitudes of $g=16.7$, $r=15.6$, $i=15.3$, and $z=15.1$ for star 12557548. From this we estimate the V magnitude is 16.2 (Windhorst et al. 1991). If we take the absolute visual magnitude of the K star to be +7.6 (with $L_s \simeq 0.14 L_\odot$), and correct for an estimated $A_V \simeq 0.22$, this puts the object at a distance of about 470 pc.

3. INTERPRETATION: GENERAL REMARKS

The data analysis presented for KIC 12557548 in the previous sections reveals a highly periodic set of occultations, likely of the 16th magnitude K-star target of this particular *Kepler* field. These occultations are highly variable in depth, and are therefore very different from anything yet reported about the other couple of thousand transiting exoplanets (including candidates).

The remarkable stability of the occultation period strongly suggests that the occultations are due to an orbital companion to KIC 12557548. In §3.1, we constrain the separation and mass of such a companion. These constraints are quite independent of any particular model. We then outline more specific scenarios to explain the variable nature of the occultations. These are: (1) direct occultations by one planet, modulated by a second planet that causes a precession of the orbital plane of the occulting planet (§3.2), and (2) dust that emanates from a single disintegrating planet (§3.3). We consider both ideas qualitatively here, and then in §4 we elaborate on the more likely one: that the occultations are due to dust emitted directly from a planetary atmosphere. In §3.4, we discuss the alternative possibility that the occultations are not of the K star, but are rather due to a low-mass eclipsing stellar binary, possibly containing an accretion disk.

3.1. Constraints on Separation and Mass of Orbital Companion

The regions of the light curve folded at the 15.685-hour period that are away from the occultations show no evidence—with a limiting amplitude of ~ 5 parts in 10^5 —for ellipsoidal light variations (ELVs) with periodicities of 15.685 hr or half that. Since the amplitudes of ELVs are of order $\text{ELV} \simeq (R_s/a)^3 (M_p/M_s)$ (where the subscript s refers to the parent star) we can set a limit on the mass of the companion M_p (assumed $< M_s$) if we have an estimate of the companion’s orbital semimajor axis a . Using the parameters for KIC 12557548 taken from the KIC, as well as our spectrum (see §2.5), we find $T_{\text{eff},s} \simeq 4400$ K, $\log g \simeq 4.63$, and $R_s \simeq 0.65 R_\odot$. These properties all point strongly toward a mid-K star of mass $M_s \simeq 0.7 M_\odot$. The semimajor axis of a small body in an assumed $P_{\text{orb}} = 15.7$ -hour orbit about such a star is

$$a \simeq 2.8 \left(\frac{M_s}{0.7 M_\odot} \right)^{1/3} R_\odot \simeq 0.013 \text{ AU}. \quad (3)$$

We then have a rather good estimate of R_s/a of 0.23. expected to make a small contribution.

When this value and our upper limit on the ELV amplitude are used in the above expression for the ELV amplitude, we obtain a constraint on the mass of the orbiting companion of

$$M_p \lesssim 3 M_J.$$

Thus, it is unlikely that the parent star has another star, or even a brown dwarf, orbiting it at a distance of only $2.8 R_\odot$.¹⁵ This leaves only planetary-mass companions as the direct or indirect cause of the occultations.

3.2. The Dual Planet Hypothesis

From our analysis in §3.1, a planet similar to Jupiter in mass and radius could be compatible with the lack of ELVs. Such a giant planet would also generate maximum eclipse depths of $\sim 1\%$, like those observed. The challenge lies in having such a Jovian-mass planet produce highly variable transit depths.

We could try to make such a model work by supposing that the transit is grazing, and that precession of the orbital plane alters the transit geometry so that the eclipse depth varies. However, orbital precession induced either by tidal distortions or by another planet in an independent orbit generally occurs over timescales much longer than the orbital period. By contrast, the eclipse depths of KIC 12557548 vary markedly from orbit to orbit. Moreover, invoking a second planet in an attempt to force rapid orbit-to-orbit variations in the planet’s trajectory across the star would result in transit timing variations (TTVs; Agol et al. 2005; Holman & Murray 2005). No TTVs are observed, although the long-cadence *Kepler* integration time hinders us from detecting TTVs substantially shorter than ~ 30 minutes. In addition, the peculiar ingress-egress asymmetry—in particular the pre-ingress brightening—evinced in the *Kepler* light curve (Figure 3) finds no ready explanation under the dual planet hypothesis.

Another way to induce precession would be to have a second planet orbit the first in a binary planet configuration (Podsiadlowski et al. 2010). However, we have verified, using the dynamical stability criteria of Mikkola (2008, and references therein), that for the parameters of KIC 12557548, two Jupiter-sized planets cannot be in a stable mutual orbit and avoid Roche lobe overflow.

3.3. Occultation by Debris from a Disintegrating Rocky Planet

Here we consider another scenario—that the occultations are produced by a much smaller, rocky planet, heated to such high temperatures that it is vaporizing. In evaporating away, it produces a debris field of dust that variably obscures up to $\sim 1\%$ of the light from the parent K star.

A purely gaseous wind emitted by a planet will not have sufficient broadband opacity to affect significantly the transit depth in the *Kepler* bandpass. For example, the hot Jupiter HD 209458b is known to emit a gaseous wind (Vidal-Madjar et al. 2003; Ben-Jaffel 2008; Linsky et al. 2010). Although this wind increases substantially the optical depth in narrow atomic absorption lines, it

¹⁵ For an assumed orbit with $P = 2 \times 15.685$ hr, and two essentially equal eclipses per orbit, the limit on the mass of the companion would be $\sim 11 M_J$ (for $M_p \ll M_s$).

hardly alters the transit depth in the broadband optical. For KIC 12557548, we must consider instead that the planetary outflow contains particulates, e.g., dust. Such dust would be driven off a rocky planet so hot that it is vaporizing. This scenario is further developed and quantified in §4.

3.4. Other Orbital Configurations

Could the source of the occultations be a low-mass eclipsing stellar binary that either is coincidentally located close on the sky to KIC 12557548 (but see the limits we have placed on blends in §2.4) or orbits KIC 12557548 in a hierarchical triple system? Such a binary might consist of, e.g., a pair of M stars, whose strongly modulated light would be diluted by light from the K star seen in KIC 12557548. If such a binary had an orbital period about the K star of $\gtrsim 10$ days, it could avoid producing a detectable ELV in the light curve of the parent star. But we know of no mechanism by which an eclipsing stellar binary like this, whether it is or is not in a hierarchical triple, can generate variable transit depths (e.g., orbital precession is too slow), let alone reproduce the transit profile shown in Figure 3 with its distinctive pre-ingress brightening and prolonged ingress.

Another possibility is that one component of the low-mass eclipsing stellar binary is a compact object, e.g., a white dwarf, fed by an accretion disk (G. Marcy, personal communication). Light from the binary, made variable by occultations of the accretion disk by the donor star, would be diluted by light from the K star. To explain the variable transit depths, the accretion disk itself would have to vary in luminosity. Why such luminosity variations would be restricted to those phases when the disk is occulted—i.e., why they would not also occur during the $\sim 70\%$ of the orbital cycle when the light curve is essentially flat—is not explained under this hypothesis.

4. OBSCURATION BY DUST FROM A DISINTEGRATING SUPER-MERCURY

In this section we examine in some detail how dust emanating from a possibly rocky planet might result in variable occultations of the parent star of up to 1.3% in depth. We discuss the size of the required dust cloud, composition and survival requirements for the dust particles, and required mass loss rates and implied lifetime of the planet against evaporation (§§4.1, 4.2, 4.3). A mechanism of ejecting gas and dust from a planet with non-negligible gravity is described in §4.4. We argue that dust can provide a natural explanation for the time variability of the mass loss and thereby of the variable occultation depths (§4.5). We carry out a numerical simulation of the motions of dust particles after they escape from the planet’s gravitational well that shows that a comet-like tail is formed, and that illustrates how the dust might scatter radiation as well as absorb it (§§4.6, 4.7). We go on to discuss how long such a close planetary system could last under the influence of tidal drag on the orbit (§4.8). Finally, we explain why occultations by dust have not been heretofore seen in other close-in, hot, rocky planets (§4.9).

A number of these sections are necessarily speculative or involve some assumptions. We offer these simply to start the thinking process on this subject rather than to provide definitive answers.

4.1. The Underlying Planet vs. the Size of the Dust Cloud

To set the stage, we assume in what follows that the planet underlying the outflow (hereafter “KIC 1255b”) has an Earth-like composition, and has mass $M_p = 0.1 M_\oplus$ (1.8 times the mass of Mercury) and radius $R_p = 0.5 R_\oplus$. In the absence of an outflow, our nominal “super-Mercury” would produce a transit depth of at most $(R_p/R_s)^2 \approx 5 \times 10^{-5}$, consistent with our lack of detections of transits in portions of the light curve. The planet’s Hill sphere radius (distance from the planet to the nearest Lagrange point) is

$$R_{\text{Hill}} = \left(\frac{M_p}{3M_s} \right)^{1/3} a \simeq 1 \times 10^9 \left(\frac{M_p}{0.1 M_\oplus} \right)^{1/3} \text{ cm}. \quad (4)$$

The Hill sphere radius is smaller than R_o , defined as the characteristic size of the occulting region during the deepest eclipses (i.e., the size of the dust cloud). We adopt a nominal value for $R_o = 0.1 R_s \simeq 5 \times 10^9$ cm, which is such that if the occulting region were circular and optically thick, it would generate a transit depth of 1%, near the maximum observed. From our experiments (not shown) simulating the occultation profile, we estimate that R_o could be a few times larger than our nominal choice if the occulting region were optically thin and/or the transit were not equatorial.

We have chosen a Mercury-like planet for our fiducial case because a low escape velocity allows us to explain how dust might be ejected. The physics of how grains can be launched successfully from a super-Mercury is explained in §4.4. In contrast, the difficulties of ejecting dust from hot rocky super-Earths are discussed in §4.9.

4.2. Dust Composition and Survival

Dayside planet temperatures peak at approximately

$$T_{\text{eff,p}} \simeq T_{\text{eff,s}} \sqrt{\frac{R_s}{a}} \simeq 2100 \text{ K}, \quad (5)$$

neglecting, among other effects, transport of heat from the substellar point by the atmosphere or by a magma ocean (see Léger et al. 2011 for an estimate of the location of the shore of the magma ocean for the hot super-Earth CoRoT-7b). Such nominal temperatures are hot enough to vaporize silicates and a variety of solid oxides, and to form a high-Z atmosphere.

This particular model requires that the atmosphere contain refractory grains which can survive for long enough to produce an observable occultation. We can think of at least two ways of loading the atmosphere with dust. The first is by condensation of dust grains from a metal-rich vapor into clouds akin to those in brown dwarf or giant planet atmospheres; see, e.g., the modeling of forsterite clouds in Cooper et al. (2003) and Madhusudhan et al. (2011). Condensation can occur where gas cools, at altitude or near the day-night terminator (Schaefer & Fegley 2009; Schaefer et al. 2011; Castan & Menou 2011). Whether such clouds can contain enough condensed mass remains to be seen—we will see in §4.3 and §4.4 that the planetary wind must contain at least as much mass in gas as in solids (or liquid droplets).

A second way to inject dust into the atmosphere is through explosive volcanism. Tidal locking of hot rocky

planets may produce a pattern of mantle convection in which volcanism is focused near the substellar point, where a thermal wind (§4.4) is best able to entrain volcanic ash (Gelman, Elkins-Tanton, & Seager 2011; van Summeren, Conrad, & Gaidos 2011). Weakening and thinning of the planetary lithosphere by sublimation may render the surface particularly vulnerable to volcanic activity. Eruptions beyond the shore of the magma ocean may be supplemented by violent bursting of bubbles at the magma ocean surface: on Earth, such eruptions can eject magma spray up to ~ 400 m/s (Taddeucci et al. 2012). Io’s plumes are a Solar System analog for volcanic injection of dust into a tenuous atmosphere; dust grain radii range from 0.03–0.12 μm (Jessup & Spencer 2012).

For completeness, we note that there might also be a third way to pepper the atmosphere with dust: as the still solid portions of the planetary surface sublime, the resulting vapor may entrain grains of more refractory composition.

The upper mantle of the Earth is composed overwhelmingly of pyroxene ($[\text{Mg,Fe}]\text{SiO}_3$) and olivine ($[\text{Mg,Fe}]_2\text{SiO}_4$). We might expect whatever grains to be present in the atmosphere of an evaporating sub-Earth to also consist of these minerals, at least in part.¹⁶ The observations of KIC 12557548 demand that grains not sublimate before they can cover up to $\sim 1\%$ of the face of the star. This requirement can be met by micron-sized grains of pyroxene, but not of olivine. In a study of grain survival times in the tails of sun-grazing comets, Kimura et al. (2002; see their Figure 4) calculated that the sublimation lifetime of an amorphous pyroxene grain having a radius $s \sim 0.2 \mu\text{m}$ is $t_{\text{sub}} \sim 3 \times 10^4$ s at a distance of $7.5 R_\odot$ from the Sun (equivalent to a distance of $2.8 R_\odot$ from the K star in KIC 12557548, neglecting the difference in the shape of the stellar spectrum heating the grain). Crystalline pyroxene survives for still longer, a consequence of its lower absorptivity at optical wavelengths and hence cooler temperature. By contrast, micron-sized grains of olivine ($[\text{Mg,Fe}]_2\text{SiO}_4$) vaporize in mere seconds.¹⁷

A sublimation lifetime of $t_{\text{sub}} \gtrsim 3 \times 10^4$ s, as is afforded by micron-sized pyroxene particles, is long enough for grains to travel the length of the occulting region. This travel time is on the order of

$$t_{\text{travel}} \sim \frac{R_{\text{Hill}}}{c_s} + \frac{R_o}{v} \sim 2 \times 10^4 \text{ s} \quad (6)$$

where the first term accounts for the time to travel from the planetary surface to the Hill sphere, and the second term accounts for the time to travel out to R_o . For the first leg of the journey, we have adopted a flow speed equal to the sound speed c_s in the planet’s high-Z atmo-

sphere:

$$c_s \simeq \sqrt{\frac{kT}{\mu m_{\text{H}}}} \simeq 0.7 \left(\frac{T}{2000 \text{ K}} \right)^{1/2} \left(\frac{30}{\mu} \right)^{1/2} \text{ km/s} \quad (7)$$

where k is Boltzmann’s constant, μ is the mean molecular weight, and m_{H} is the mass of hydrogen. The sound speed is appropriate to use if the grains are carried off the planetary surface by a thermal Parker-type wind, as discussed in §4.4. For the second leg of the journey, we adopt $v \sim 10$ km/s. This is a characteristic grain velocity once the wind is rarefied enough that dust decouples from gas, and is given by the dynamics dictated by gravity and radiation pressure (see §4.6).

4.3. Mass Loss Rate and Evaporation Timescale

The mass loss rate in dust grains may be estimated as

$$\dot{M}_d \simeq \Omega \rho_d v R_o^2 \quad (8)$$

where ρ_d is the mass density in dust grains at a distance R_o from the planet,¹⁸ v is the outflow velocity (on scales of R_o), and Ω is the solid angle subtended by the flow as measured from the planet center. We can relate ρ_d to the optical depth through the dust flow, integrated along the line-of-sight path of length $\mathcal{R} \sim R_o$:

$$\tau \simeq \rho_d \mathcal{R} \kappa_d \sim \frac{\rho_d R_o}{\rho_b s} \quad (9)$$

where the dust opacity $\kappa_d \sim s^2/(\rho_b s^3) \sim 1/(\rho_b s)$ for grains of radius s and bulk density $\rho_b \sim 3 \text{ g cm}^{-3}$. We can also relate τ to the eclipse depth f , assuming $\tau \lesssim 1$ (we will discuss why the flow may be optically thin, or marginally so, in §4.5):

$$f \sim \frac{\tau R_o^2}{R_s^2} \sim 0.01 \left(\frac{\tau}{1} \right) \left(\frac{R_o/R_s}{0.1} \right)^2. \quad (10)$$

Combining the above three relations, we have

$$\begin{aligned} \dot{M}_d &\sim \frac{\Omega \rho_b s f R_s^2 v}{R_o} \simeq 2 \times 10^{11} \left(\frac{\Omega}{1} \right) \left(\frac{\rho_b}{3 \text{ g/cm}^3} \right) \left(\frac{s}{0.2 \mu\text{m}} \right) \\ &\times \left(\frac{f}{0.01} \right) \left(\frac{v}{10 \text{ km/s}} \right) \left(\frac{0.1}{R_o/R_s} \right) \left(\frac{R_s}{0.65 R_\odot} \right) \text{ g/s} \\ &\simeq 1 M_\oplus/\text{Gyr} \end{aligned} \quad (11)$$

where Ω is normalized to 1 to account for the likelihood that the area from which dust is launched may primarily be in the substellar region. If, as noted in §4.1, $\tau \lesssim 1$ and/or the transit is not equatorial, then R_o may be up to a few times larger than $0.1 R_s$, and the above estimate of \dot{M}_d would need to be reduced somewhat.

Gas (metal-rich vapor) adds to the total mass loss rate by a factor of ξ . If we assume that the mass loss mechanism principally produces a gaseous outflow, and that drag accelerates the dust grains, then it seems reasonable to assume that the gas density must be at least as large as the dust density: $\xi \gtrsim 2$. Otherwise the backreaction drag on gas by dust would slow the gas down and prevent it from escaping. We will revisit the factor of ξ more

¹⁶ Another possibility involves grains of alumina (a.k.a. corundum; Al_2O_3), which seems likely if the planetary surface has been distilled to the point where it is composed predominantly of calcium-aluminum oxides (see Figure 5 of Léger et al. 2011).

¹⁷ We have been unable to identify a simple reason why the sublimation times of olivine grains are orders of magnitude shorter than those of pyroxene grains; see references in Kimura et al. (2002) for the original laboratory data.

¹⁸ For this back-of-the-envelope estimate, we neglect the difference between the planet center and the center of the dust cloud.

quantitatively in §4.4; for now, we note that $\xi \sim 2$ falls squarely in the range of values inferred for cometary outflows of dust mixed with gas (Delsemme 1982; Fernandez 2005). Then the evaporation timescale for our nominal $M_p = 0.1 M_\oplus$ planet is

$$t_{\text{evap}} \sim \frac{M_p}{\mathcal{F} \xi \dot{M}_d} \sim 0.2 \left(\frac{0.3}{\mathcal{F}} \right) \left(\frac{2}{\xi} \right) \text{ Gyr} \quad (12)$$

where \mathcal{F} is the fraction of time the planet spends losing mass at the maximum rate (set by $f = 0.01$). Our estimate of t_{evap} is nominally shorter than the likely age of the star, but not by an implausibly large factor.

4.4. Ejecting Dust Grains Via a Thermal Wind

In this section, we explore the possibility that dust is ejected from KIC 1255b in a manner that resembles dust ejection from comets (for a pedagogical review of comets, see Rauer 2007). Gas sublimates and then flows off a comet nucleus at essentially the sound speed, which can be dozens of times greater than the escape velocity from the nucleus. As gas atoms stream toward the cometopause—the surface of pressure balance between cometary gas and the Solar wind—they are photoionized by stellar ultraviolet photons. At the cometopause, cometary ions are rapidly picked up by the magnetic field of the Solar wind, and accelerated up to the Solar wind speed of hundreds of km/s. This explains the well-known observation that the ionized gas tails of comets are swept anti-Sunward, in the direction of the Solar wind. Sufficiently small dust particles, on the other hand, escape the nucleus by virtue of the hydrodynamic drag exerted by the escaping gas.

An important difference between a comet and KIC 1255b is the much higher surface gravity of our nominal super-Mercury. The surface escape velocity

$$v_{\text{esc,surf}} \simeq 5 \left(\frac{M_p}{0.1 M_\oplus} \right)^{1/2} \left(\frac{0.5 R_\oplus}{R_p} \right)^{1/2} \text{ km s}^{-1} \quad (13)$$

is ~ 7 times higher than the local sound speed c_s . At first glance, then, it seems unlikely that gas can be driven off the surface of the planet. But in Parker-type winds (see, e.g., Lamers & Cassinelli 1999) the base of the wind can be characterized by just such values of $v_{\text{esc,surf}}/c_s$. Starting at their base, Parker-type winds accelerate by gas pressure over long distances—several planetary radii—before the bulk wind speed v formally exceeds the *local* escape velocity. For example, $v_{\text{esc,surf}}/c_s \sim 5$ in the Solar corona, which is the seat of the Solar wind (e.g., Lemaire 2011). Another example is provided by the thermal winds from hot Jupiters, where $v_{\text{esc,surf}}/c_s \sim 5$ at the base of the planetary wind where stellar UV photons are absorbed and heat the upper atmosphere (e.g., Murray-Clay, Chiang, & Murray 2009). Note that both these examples represent flows that are continuously heated and energized along their extents—by photoionization in the case of the hot Jupiter wind, and by conduction and wave heating in the case of the Solar wind (e.g., Marsch, Axford, & McKenzie 2003). Thus these winds can remain nearly in the hydrodynamic regime and enjoy large mass fluxes, even at the large Jeans parameters ($\lambda_0 \equiv v_{\text{esc}}^2/2c_s^2$) characterizing their base radii R_{base} .¹⁹

¹⁹ To quantify this statement, note that a hot Jupiter wind

The thermal winds noted above suggest by analogy that the atmosphere of KIC 1255b can be gradually accelerated by gas pressure to speeds that eventually exceed the local escape velocity. Gas can be continuously heated along the extent of the wind by collisions with grains, which in turn are heated by starlight; thus the wind should maintain a nearly constant temperature $\gtrsim 2000$ K. At distances of $R_{\text{Hill}} \sim 3R_p$, near the first and second Lagrange points where the effective gravitational acceleration is nearly zero, we anticipate that the outflow will have attained the sonic point, so that the wind velocity will be of order c_s on these scales (see, e.g., Figure 9 of Murray-Clay et al. 2009). This explains the first term in equation 6. Of course, this sketch needs to be confirmed with a first-principles calculation of the mass loss rate as a function of planet mass.

How dense and fast must the gaseous outflow be to lift grains off the surface of the planet? The aerodynamic drag force on a grain must exceed the force of planetary gravity:

$$\rho_g v_g c_s s^2 \gtrsim \rho_b s^3 g \quad (14)$$

where $g \sim 400 \text{ cm s}^{-2}$ is the surface gravitational acceleration, and ρ_g and v_g are the gas density and flow velocity, respectively. For the drag force on the left-hand side we have used the Epstein (free molecular) drag law, appropriate for grains whose sizes are less than the collisional mean free path between gas molecules, and for flow velocities $v_g \lesssim c_s$ (Epstein 1924). Both of these conditions can be verified *a posteriori* to hold throughout the flow. The atmospheric density just above the ocean melt is $\rho_g \sim P/c_s^2$, where the surface pressure $P \sim 10 \mu\text{bar}$ at $T = 2100 \text{ K}$, if the ocean is composed predominantly of Mg, Si, and O, with zero contribution from Na (see Figures 5 and 6 from Léger et al. 2011, and consider vaporized fractions $0.85 > F_{\text{vap}} > 0.02$; see also Schaefer & Fegley 2009). Such an atmosphere is composed primarily of Mg, SiO, O, and O₂ gas, according to Figure 3 of Schaefer & Fegley (2009). Then the vertical wind velocity required to keep grains aloft against gravity is

$$v_g \gtrsim 2 \left(\frac{10 \mu\text{bar}}{P} \right) \left(\frac{s}{0.2 \mu\text{m}} \right) \text{ m/s} \quad (15)$$

which seems easy to satisfy. If the surface has been vaporized (distilled) to the point where it is composed of Al, Ca, and O ($F_{\text{vap}} > 0.85$), then $P \sim 0.1 \mu\text{bar}$ and $v_g \gtrsim 200 \text{ m/s}$, which still seems possible (at least horizontal wind velocities are thought to have near-sonic velocities; Castan & Menou 2011).

The lift-off condition (14) implies a mass loss rate in *gas* of

$$\dot{M}_g \sim \Omega \rho_g v_g R_p^2 \gtrsim 4 \times 10^{10} \left(\frac{\Omega}{1} \right) \left(\frac{s}{0.2 \mu\text{m}} \right) \text{ g/s}. \quad (16)$$

(as computed, e.g., in the standard model of Murray-Clay et al. 2009) is characterized by $\Phi/\Phi_{0,0} \approx 0.05$ at $\lambda_0 \approx 13.5$, in the notation of Volkov et al. (2011). Here $\Phi/\Phi_{0,0}$ is the dimensionless mass loss rate, and the “0” base radius is taken to be the surface which presents unit optical depth to UV photons. For comparison, Volkov et al. (2011), who neglect energy deposition at radii $> R_{\text{base}}$, predict $\Phi/\Phi_{0,0} \approx 4 \times 10^{-5}$ at $\lambda_0 = 13.5$ (see their Figure 3). Thus the continuous energy deposition enjoyed by a hot Jupiter wind increases the mass loss rate above what it would be without continuous energy deposition by about three orders of magnitude.

The fact that the minimum value of \dot{M}_g is comparable to \dot{M}_d as estimated in (11) supports our claim in §4.3 that the gas-to-dust ratio may be of order unity, i.e., $\xi \sim 2$.

It is remarkable that at a maximum eclipse depth $f = 0.01$, our order-of-magnitude estimate for the total mass loss rate $\xi \dot{M}_d \sim 4 \times 10^{11}$ g/s from our super-Mercury either matches or exceeds, by up to an order of magnitude, estimates of mass loss rates—mostly in hydrogen gas—from hot Jupiters like HD 209458b (Vidal-Madjar et al. 2003; Yelle 2004; Garcia-Munoz 2007; Murray-Clay et al. 2009; Linsky et al. 2010) and HD 189733b (Lecavelier des Etangs et al. 2010). Hot Jupiters are thought to lose mass by photoevaporation, whereby stellar X-ray and ultraviolet (XUV) radiation photoionizes, heats, and drives a thermal wind off the uppermost layers of a planetary atmosphere. Present-day mass loss rates of hot Jupiters are limited by the XUV luminosities of main-sequence solar-type stars, of order $L_{\text{XUV},s} \sim 10^{-5} - 10^{-6} L_\odot$. In the case of KIC 1255b, mass loss may also be driven by a thermal wind—but one which is powered by the bolometric stellar luminosity, $L_s \sim 0.14 L_\odot$, which heats the entire planetary atmosphere to temperatures $T \simeq 2000$ K. The power required to drive our inferred mass loss rate

$$\begin{aligned} L_{\text{required}} &= \frac{GM_p \xi \dot{M}_d}{R_p} \\ &\sim 6 \times 10^{22} \left(\frac{\xi}{2} \right) \left(\frac{s}{0.2 \mu\text{m}} \right) \left(\frac{\tau}{1} \right) \text{ erg/s}, \end{aligned} \quad (17)$$

(G is the gravitational constant) is easily supplied by the total power intercepted in stellar radiation,

$$L_{\text{intercepted}} = \frac{L_s}{4\pi a^2} \cdot \pi R_p^2 \sim 4 \times 10^{26} \text{ erg/s}. \quad (18)$$

4.5. Time Variability of Mass Loss and Limiting Mass Loss Rate

The variability observed in the obscuration depths implies substantial changes in \dot{M}_d (or in other physical properties of the outflowing dust clouds) over timescales $\lesssim P_{\text{orb}} = 15.7$ hr. Although we cannot be quantitative, such rapid variability seems possible to accommodate within the framework of an evaporating planet. Again, a comparison with comets is instructive. As in a cometary nucleus, inhomogeneities or localized weaknesses in the planet's surface ("vents"; Jewitt 1996; Hsieh et al. 2010) may cause the planet to erupt occasionally in bursts of dust. Whatever gas is ejected from the planet will be photoionized by the stellar radiation field and, like the gas tails of comets, interact with the magnetized stellar wind. To the extent that dust can be entrained in plasma along the planet's magnetotail, plasma instabilities may introduce further time variability.

The mass loss rate \dot{M}_d may be limited to $\sim 2 \times 10^{11}$ g s^{-1} , the value in equation (11) appropriate to an optical depth $\tau \sim 1$ (assuming all other parameters in that equation are fixed at their nominal values). This upper limit exists because if the flow became too optically thick, light from the star would not reach the planet's surface to heat it. Thus the mass loss rate may be self-limiting in a way that keeps the outflow from becoming too optically

thick. One can imagine a limit cycle which alternates between a low-obscuration phase during which starlight strikes the planet's surface directly and dust proceeds to load the planet's atmosphere, and a high-obscuration phase during which dust removal dominates production.

Wind mass loss rates should depend on outgassing rates from the planetary surface. Since saturation vapor pressures depend exponentially on temperature, it seems easy to imagine that modest changes in surface temperature due to changes in the optical depth of the wind will drive large changes in \dot{M}_d . As noted above, a first-principles calculation of \dot{M}_d along the lines of the externally irradiated solution for hot Jupiter winds (e.g., Murray-Clay et al. 2009) would be welcome.

4.6. Dust Stream Structure

Once dust escapes from the planet, and the gas density becomes too low to exert significant drag, the dust will be swept back into a comet-like tail by the combination of radiation pressure and Coriolis forces. The ratio of the stellar radiation pressure force on a grain to that of stellar gravity equals

$$\begin{aligned} \beta &\equiv \frac{F_{\text{rad}}}{F_{\text{grav},s}} = \frac{3Q_{\text{pr}}L_s}{16\pi GcM_s\rho_b s} \\ &\simeq 0.15 \left(\frac{L_s}{0.14 L_\odot} \right) \left(\frac{0.7 M_\odot}{M_s} \right) \left(\frac{0.2 \mu\text{m}}{s} \right) \end{aligned} \quad (19)$$

where Q_{pr} is the radiation pressure efficiency factor (see, e.g., Burns et al. 1979) and c is the speed of light. For the numerical evaluation in (19), we have used the results of Kimura et al. (2002, their Figure 2) for a spherical pyroxene particle, scaled for the luminosity and mass of our K star. The numerical result in (19) is valid only for $s \gtrsim 0.2 \mu\text{m}$ (as s decreases below $0.2 \mu\text{m}$, Q_{pr} decreases and radiation pressure is increasingly negligible; in any case such grains are unimportant because they sublimate too quickly).

We performed a simple calculation of what a dust tail might look like. Since the precise details of how dust is launched from the surface are presently unclear—they are subject, e.g., to horizontal winds on the planet that can distribute material from the substellar point to the nightside—the calculation simply assumes a spherically symmetric outflow of dust from the planet at the surface escape speed. Our fiducial planet parameters of $R_p = 0.5 R_\oplus$ and $M_p = 0.1 M_\oplus$, $\beta = 0.15$, and a sublimation time for the dust of $t_{\text{sub}} = 10^4$ s were assumed. The computations were performed in a frame of reference rotating with the planet's orbit, and followed 30,000 dust particles from launch to sublimation.

The results of this simulation are shown in Fig. 6. A long dust tail is apparent because the color scaling covers a large dynamic range of column densities. The effective length of the tail is not actually that long, e.g., the column density of dust particles is quite small at distances comparable to R_s . This was quantified by integrating the total number of dust grains within $\pm 1/8$ of the stellar radius in height (z) as a function of distance along the dust tail (y). The result is shown in Fig. 7. Given the presently available information, only relative values of the optical depth can be shown, but the curve serves to show that the projected density of dust grains falls

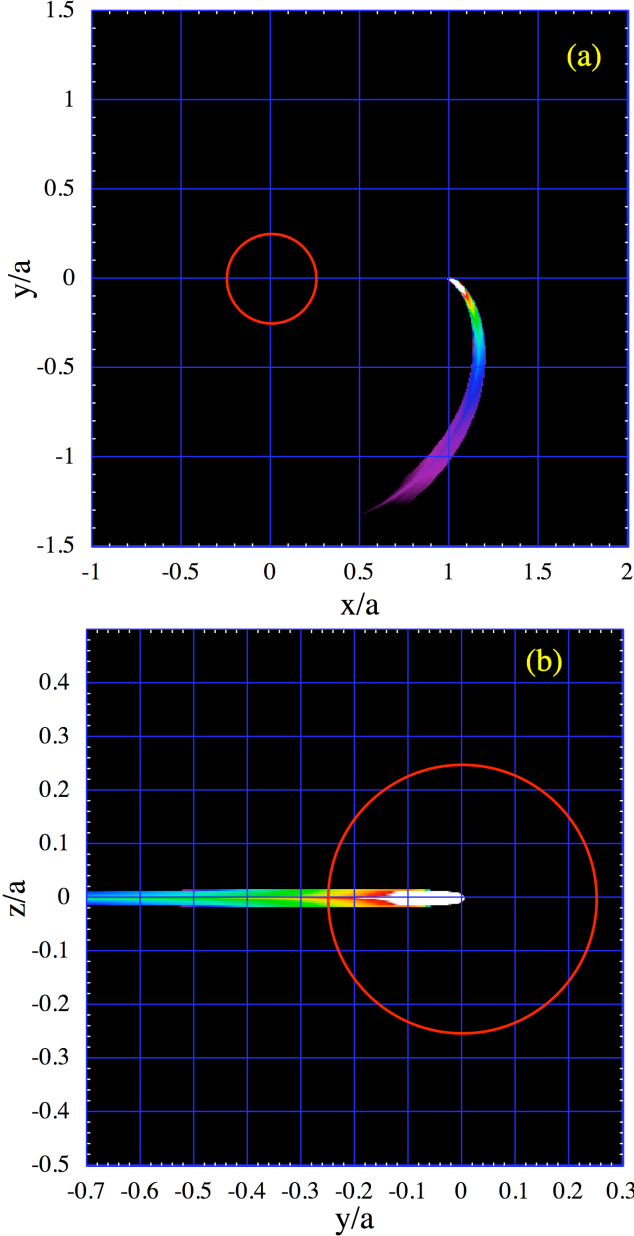


Figure 6. Simulations of dust flows from a $0.1 M_{\oplus}$ planet of $0.5 R_{\oplus}$ driven by radiation pressure from the parent star. The spatial scale is in units of the semimajor axis of the planet. The color scale is proportional to the square root of the projected density in order to enhance the dynamic range. The red circle represents the parent star. The top panel shows the dust density as viewed from the orbital pole; the bottom panel shows the dust density as seen by an equatorial observer at mid transit.

off sharply with distance from the planet. Thus, the optical depth could be somewhat greater than unity near the projected planet disk, and the net obscuration of the parent star could take on values up to the maximum level of $\sim 1.3\%$ that is observed.

In summary, the dust stream geometry seems able to accommodate the occultation durations and depths. It might even be able to explain the curious ingress-egress asymmetry in the occultation profile, as we argue in the next section.

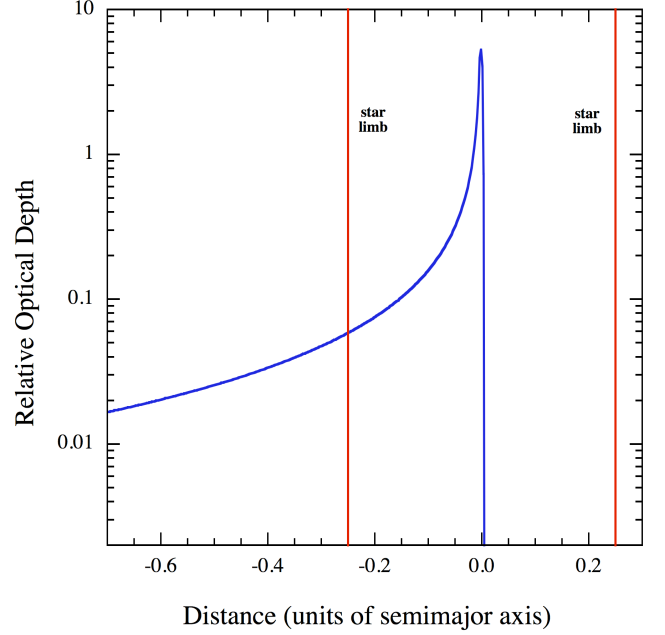


Figure 7. Relative optical depth of the simulated dust tail as a function of distance across the parent star in units of the semimajor axis. This result is derived from the simulated data used to produce Fig. 6. The vertical scale is arbitrary since otherwise we would need to know the absolute value of the optical depth near the surface of the planet.

4.7. Scattering

The putative dust cloud likely attenuates more by scattering photons out of our line of sight than by actual absorption (this is due to the small imaginary part of the index of refraction in the visible; see, e.g., Denevi et al. 2007). This opens the possibility that scattering of starlight into the line of sight would produce, at certain orbital phases, an *excess* of light above the nominal out-of-occultation region levels. An excess would be more likely given the presence of larger ($s \gtrsim 1 \mu\text{m}$) grains that scatter primarily in the forward direction.

We can estimate the ratio of fluxes scattered into, versus out of, our line of sight. Consider an idealized, small, spherical scattering cloud of radius R_d that scatters a fraction A (for “albedo”) of all the stellar radiation incident upon it (i.e., the cloud presents a total scattering cross section of $A \cdot \pi R_d^2$). The incident radiation is scattered uniformly into a solid angle Ω_{scat} centered about the direction of the incident beam. In the case that the cloud sits directly in front of the target star, the ratio of fluxes scattered into, versus out of, the line of sight is

$$\frac{\chi_{\text{in}}}{\chi_{\text{out}}} \simeq \frac{\pi}{\Omega_{\text{scat}}} \left(\frac{R_s}{a} \right)^2 \simeq \frac{\pi}{16 \Omega_{\text{scat}}} \quad (20)$$

independent of A and R_d . The ratio ranges from $\sim 1.6\%$ for isotropic scattering, to as high as $\sim 20\%$ for forward scattering into 1 steradian. If the dust cloud is blocking the stellar disk, then attenuation is dominant (except in the case of extreme forward scattering). However, if the dust cloud is not blocking the stellar disk, then there may be a small excess contribution to the system light. This may explain the small bump in flux just before ingress, and the small depression in the flux just after egress (see

Fig. 3). In this interpretation, the ingress-egress asymmetry results from the asymmetric distribution of dust in the planetary outflow. Just prior to ingress, light is forward-scattered off the dusty head of the “comet” into our line of sight, producing the small bump in flux. Light may continue to be forward scattered into the line of sight during the main occultation and even after egress. However, at those phases when part of the tail occults the star, the scattering of starlight out of the line of sight is likely to dominate and produce a net depression in the observed intensity.

4.8. Tidal Inspiral Lifetime

We now consider how long such a planet as the one we are proposing might last in the face of tidal decay due to interactions with the parent star. The timescale of tidal decay is approximately

$$\tau_{\text{tidal}} \simeq Q \frac{2M_s}{9M_p} \left(\frac{a}{R_s} \right)^5 \frac{P_{\text{orb}}}{2\pi} \simeq 10^{10} \left(\frac{Q}{10^6} \right) \text{ yr} \quad (21)$$

(see, e.g., Gu, Lin, & Bodenheimer 2003) where Q is the usual dimensionless measure of dissipation in the parent star, and we have assumed that the parent star is rotating with an angular frequency much lower than the planet’s orbital frequency, and that the orbital eccentricity is zero. Thus, even for a pessimistically small value of Q , the lifetime against tidal decay is more than adequately long.

4.9. Differences Between KIC 12557548 and Hot Super-Earths

If our proposed scenario for KIC 1255b is correct, why don’t other hot rocky planets also evince occulting dust clouds? The class of close-in rocky planets includes CoRoT-7b (Léger et al. 2009; Léger et al. 2011), 55 Cnc e (Winn et al. 2011), and Kepler-10b (Batalha et al. 2011b).²⁰ All are argued to have significant rock components, although an admixture of water, hydrogen, and/or other light elements seems required to explain 55 Cnc e.

The primary parameter distinguishing the super-Mercury that we are imagining orbits KIC 12557548 and the other hot rocky planets is clearly the planet mass. All the other planets are “super-Earths” having masses $M_p \simeq 10 M_\oplus$ and radii $R_p \simeq 2 R_\oplus$ (mass-radius relations for super-Earths, may be found in, e.g., Valencia et al. 2007 or Figure 3 of Winn et al. 2011). Super-Earths have surface escape velocities that, at $v_{\text{esc},p} \simeq 25 \text{ km/s}$, are almost certainly too large for gas that is heated to temperatures $T \simeq 2000\text{--}3000 \text{ K}$ to escape at substantial rates via Parker-type winds. The efficiency of driving a thermal wind drops rapidly with increasing $v_{\text{esc},p}$. The local hydrostatic scale height of gas (valid for altitudes $h \lesssim R_p$)

$$h_{\text{scl}} \sim \frac{2c_s^2}{v_{\text{esc}}^2} R_p \sim 2 \times 10^{-3} \left(\frac{30}{\mu} \right) \left(\frac{10M_\oplus}{M_p} \right) \left(\frac{R_p}{2R_\oplus} \right) R_p \quad (22)$$

²⁰ Kepler-9d (Batalha et al. 2011a) may also belong to this class based on its size and orbital distance, but, unfortunately, its mass is not yet known, and therefore we cannot be sure that it is a purely rocky planet.

decreases as $1/v_{\text{esc}}^2$. For super-Earths, the base of a Parker-type wind (the base is roughly identified as that location where the local value of $v_{\text{esc}}/c_s \sim 6$) would lie several R_p away from the planetary surface, while for a super-Mercury the base would lie close to the surface. Because the gas density must decrease more or less according to $\rho_g \propto \exp(-h/h_{\text{scl}})$ from the surface to the base, the gas density at the base on a super-Earth would be many orders of magnitude lower than on a super-Mercury.

Alternate mechanisms of mass loss from super-Earths, other than a Parker-type wind, include: (i) XUV photoevaporation (by analogy with hot Jupiters), (ii) stellar wind drag, and (iii) stellar radiation pressure. All fail to explain the inferred mass loss rates for KIC 1255b. The intercepted power from the stellar XUV luminosity is at least a factor of 10 too low compared to L_{required} (see equation 17), even for optimistically high values of $L_{\text{XUV},s} = 10^{-5} L_\odot$ and of the efficiency $\varepsilon = 0.1$ with which XUV photon energy is converted to mechanical work.^{21,22} Stellar wind drag suffers the same problem that XUV photoevaporation does: the power intercepted by the planet from the stellar wind is insufficient to supply L_{required} . An easy way to see this is to note that the mechanical luminosity of the Solar wind is $L_{\text{wind},s} \sim (1/2) \dot{M}_\odot v_{\text{wind},s}^2 \sim (1/2) \cdot (2 \times 10^{-14} M_\odot/\text{yr}) \cdot (400 \text{ km/s})^2 \sim 3 \times 10^{-7} L_\odot < L_{\text{XUV},s}$.^{23,24} The intercepted power is still too low even were we to account for a planetary magnetosphere, which would increase the cross section presented by the planet by a factor $\lesssim 10$.²⁵ Finally, based on the calculations of Kimura et al. (2002), the force of stellar radiation pressure acting on a grain is at most $\sim 30\%$ of the force of planetary gravity on a super-Earth, for conditions in KIC 12557548 (but see §§4.6–4.7). Moreover, even if the force of radiation pressure on a grain were somewhat larger than that of planetary gravity, the grain would be dragged by ambient gas, and might never accelerate to escape velocity.

For all these reasons, super-Earths cannot launch dusty outflows like those we infer for KIC 12557548—whereas sub-Earths can. There is still another reason why dust clouds are especially observable for KIC 12557548 and not in the other observed systems. Even if dust grains could be driven off the hot super-Earths detected to date, they would be too hot; grains in these other systems would sublimate too quickly to travel far from their parent planets, and would fail to block as much light from their host stars. If we use equation (5) to estimate the temperature of a grain at the location of each super-

²¹ XUV luminosities of K dwarfs are typically $3 \times$ greater than those of G dwarfs (Hodgkin & Pyle 1994; Lecavelier des Etangs 2007).

²² The efficiency ε is lowered by ionization and radiative losses; radiative losses may be especially severe in the case of KIC 1255b because of cooling by dust, a problem that does not afflict hot Jupiter winds.

²³ Mass loss rates of K stars are observed to be comparable to that of the Sun (Wood et al. 2005; Cranmer 2008).

²⁴ At the orbital distance of KIC 1255b, the energy carried by the stellar wind is mostly magnetic and thermal, not kinetic. But after accounting for all three forms of energy using empirical measurements of the Solar wind at $a = 2.8 R_\odot$, we arrived at roughly the same total power output, $L_{\text{wind},s} \sim 10^{-6} L_\odot$.

²⁵ If KIC 1255b has a surface dipole field of 1 G, then its magnetospheric radius is $\sim 2 R_p$.

Earth, we find:

- Kepler-10b : 3000 K
- 55 Cnc e : 2800 K
- CoRoT-7b : 2500 K
- KIC 1255b : 2100 K

Thus KIC 1255b—orbiting the coolest star—is distinguished in having the coolest grains. Sublimation lifetimes t_{sub} are exponentially sensitive to temperature. For example, whereas we have estimated $t_{\text{sub}} \sim 3 \times 10^4$ s for 0.2- μm -sized pyroxene grains emitted by KIC 1255b, these same grains emitted by CoRoT-7b would have $t_{\text{sub}} \sim 10^2$ s (Kimura et al. 2002)—considerably shorter than the travel time $t_{\text{travel}} \sim 2 \times 10^4$ s required to produce a $\sim 1\%$ occultation (§4.2).

Thus KIC 1255b apparently occupies a sweet spot for the production of occulting dust clouds: the system is hot enough for the surface to vaporize and for a wind to be launched,²⁶ but cool enough that dust particles can be formed from certain minerals not quite hot enough to vaporize (or to form by condensation upon cooling of the vapor after it flows to a different location), and to allow these dust particles to travel a significant fraction of the host stellar radius.

5. SUMMARY AND OUTLOOK

We have reported on occultations of KIC 12557548 that recur with a period of 15.6854 hours, have depths that range from 1.3% to $\lesssim 0.15\%$, and that vary on timescales comparable to, if not also shorter than, the occultation period. A search for periodic modulation in the depths of the occultations did not reveal anything definitive. From various lines of evidence, most notably a newly acquired optical spectrum, the target star appears to be a mid-K dwarf.

We briefly considered a scenario wherein the changing transit depths are due to a dual giant planet system (either on separate orbits or in a binary pair) in which one of the planets undergoes grazing transits of the target K star. The orbital plane of the transiting planet would have to precess in such a way as to effect the variable occultation depths. We find, however, that a binary planet configuration is very likely to be dynamically unstable, even if the two planets are themselves essentially in a contact configuration. In the case of two planets on separate orbits, it is not clear how orbital precession could explain either the remarkable changes from orbit to orbit or the long intervals of ~ 10 and 20 days when the occultations mostly disappear. We also briefly considered an eclipsing binary that is orbiting KIC 12557548 in a hierarchical triple configuration, but were unable to explain the basic properties of the observed light curve in the context of such a scenario.

We come down in favor of a scenario in which dust is aerodynamically dragged off an orbiting rocky planet—possibly one not much larger than Mercury in size—by a thermal Parker-type wind composed of metal atoms sublimated off the planet’s surface at a temperature of

~ 2000 K. The atmosphere may be loaded with dust either through condensation into clouds, or through explosive volcanic activity. The mass loss rate must sometimes be as high as a few times 10^{11} g/s, or about $1 M_{\oplus}/\text{Gyr}$, and may comprise by mass roughly equal parts gas and dust. Our fiducial mass and radius for the underlying planet are $0.1 M_{\oplus}$ and $0.5 R_{\oplus}$, respectively. The corresponding lifetime against evaporation is ~ 0.2 Gyr. This is probably less than the age of the star, but is not alarmingly short. Because the mass loss rates are inferred from the observations and as such are largely fixed, planets much smaller in mass than our fiducial super-Mercury have implausibly short evaporation lifetimes, while planets much larger in mass and thus in surface gravity do not seem capable of sustaining the required mass loss rates.

After leaving the planet’s gravitational well, the dusty gas will soon become rarified to the point that the dust and gas trajectories diverge. We have simulated how dust grains, decoupled from gas, would be shaped into a comet-like tail by the Coriolis force and stellar radiation pressure. The head-tail asymmetry of the dust cloud promises to explain the observed ingress-egress asymmetry in the occultation profile. Pyroxene grains, each a fraction of a micron in size, are a good candidate for the obscuring grains because of their relatively long lifetimes against sublimation—alumina is also a promising high-temperature mineral to consider. Time variability of the outflow’s dust density as reflected in time variability of the occultation depths could be caused by any number of factors: irregularities and uneven outgassing rates on the planet’s possibly volcanic surface; a feedback loop between mass loss and the stellar radiation flux received at the planet’s surface that causes both to fluctuate with time; and instabilities resulting from the interaction of the ionized planetary wind with the magnetized stellar wind. The analogy between our evaporating super-Mercury and comets may not be a bad one, but much theoretical work remains to be done to put this scenario on a more quantitative and secure footing.

5.1. Observational Prospects

Obviously, short-cadence observations with *Kepler* would be helpful in clarifying the issue of whether there are shape changes in individual occultations vs. only changes in the overall depths. Some shape changes would be expected, as the timescale for the wind to “refresh” is given by the grain travel time $t_{\text{travel}} \sim 5$ hr (equation 6), which is not much longer than the eclipse duration of 1.5 hr. The target star, at $K_p = 15.7$ magnitudes, is not very bright, but each 1-minute sample with *Kepler* would yield $1\sigma \sim 0.15\%$ counting statistics. Given that the depths of the deepest occultations are 1.3%, this would provide a signal-to-noise of 8:1 for individual samples. The ingress and egress should be resolved in short-cadence data and the shapes should give important clues as to the nature of the system.

Observations with a large optical/infrared telescope, either from the ground or from space, would also prove helpful. Measurement of the wavelength dependence of the occultation depth could confirm our hypothesis that sub-micron-sized dust is responsible. The detection of solid-state absorption features (e.g., the 10 μm silicate band) would also clinch the case for dust. Deep imaging

²⁶ The three sub-Earths orbiting KOI-961 (Muirhead et al. 2012) are probably too cold to satisfy this condition.

would have the added benefit of further ruling out blends with faint, variable interlopers.

Searching for extra in-transit absorption by metals—e.g., photoionized Mg, O, Si, Ca, and Fe—through observations of spectral lines could lead to a direct demonstration that the underlying planet is comprised largely of heavy elements, and is evaporating (cf. Linsky et al. 2010). Our rough calculations indicate that in some lines (e.g., the Mg II 2800 Å doublet), the gaseous outflow may be so optically thick that its occulting size is limited only by the confining pressure of the incident stellar wind. We estimate the corresponding maximum flux decrement in any spectral lines to be on the order of ~5%.

If there indeed turns out to be a super-Mercury orbiting KIC 12557548, where the occultations are due to dust carried by outflowing sublimated gas, the planet would be among the smallest-mass bodies ever to have been (indirectly) detected. It would be the first extrasolar planet shown to be geologically active and to be disintegrating via the loss of high-Z material.

We thank the anonymous referee for an encouraging and incisive report that motivated us to consider volcanic activity and to examine more quantitatively the ability of the atmosphere to entrain solids; Raymond Jeanloz and Michael Manga for instructive exchanges about vaporizing silicates and volcano ejecta speeds; Josh Carter for discussions about data validations and the viability of a dynamically stable binary planet; Ruth Murray-Clay for input about thermal winds; Robert Szabo for information about properties of RR Lyrae stars; and Bryce Croll, Dan Fabrycky, Ron Gilliland, Meredith Hughes, John Johnson, Heather Knutson, Tim Morton, Margaret Pan, Erik Petigura, and Josh Winn for stimulating discussions about follow-up observations. We consulted with Ron Remillard, Rob Simcoe, and Adam Burgasser about spectral classifications. We would also like to thank Robert Lamontagne and the staff at the Observatoire Astronomique du Mont-Mégantic for their assistance. EC is grateful for support from the National Science Foundation, and for useful and encouraging feedback from participants of the Berkeley Planet and Star Formation Seminar, including Ryan O’Leary and Geoff Marcy who shared their own analyses of the *Kepler* data on KIC 12557548. LN thanks the Natural Sciences and Engineering Research Council (NSERC) of Canada for financial support. BK is grateful to the MIT Kavli Institute for Astrophysics and Space Research for the hospitality they extended during her visit and the support provided by the Turkish Council of Higher Education.

REFERENCES

- Agol, E., Steffen, J., Sari, R., & Clarkson, W. 2005, *MNRAS*, 359, 567
 Batalha, N., et al. 2010, *ApJ*, 713, L10
 Batalha, N., et al. 2011a, *ApJ*, 727, 24
 Batalha, N., et al. 2011b, *ApJ*, 729, 27
 Batygin, K., Stevenson, D.J., & Bodenheimer, P.H. 2011, *ApJ*, 738, 1
 Ben-Jaffel, L. 2008, *ApJ*, 688, 1352
 Borucki, W. J., et al. 2011, *ApJ*, 736, 19
 Burns, J.A., Lamy, P.L., & Soter, S. 1979, *Icarus*, 40, 1
 Castan, T. & Menou, K. 2011, *ApJ*, 743, 36
 Cooper, C.S., Sudarsky, D., Milsom, J.A., Lunine, J.I., & Burrows, A. 2003, *ApJ*, 586, 1320
 Cranmer, S.R. 2008, *ASP Conference Series*, 14th Cambridge Workshop on Cool Stars, Stellar Systems, and the Sun, 384, 317
 Dawson, R.I., & Fabrycky, D.C. *ApJ*, 2010, 722, 937
 Delsemme, A.H. 1982, *Icarus*, 49, 438
 Denevi, B.W., Lucey, P.G., Hochberg, E.J., & Steutel, D. 2007, *JGR*, 112, E05009
 Epstein, P.S. 1924, *Physical Review*, 23, 710
 Fernandez, J.A. 2005, *Comets: Nature, Dynamics, Origin, and Their Cosmogonical Relevance*, (Springer Science & Business)
 Fischer, D.A., et al. 2008, *ApJ*, 675, 790.
 García-Muñoz, A. 2007, *P&SS*, 55, 1426
 Gelman, S. E., Elkins-Tanton, L. T., & Seager, S. 2011, *ApJ*, 735, 72
 Gu, P.-G., Bodenheimer, P.H., & Lin, D.C. 2003b, *ApJ*, 588, 509
 Harrington, R.S. 1972, *Cel. Mech.*, 6, 322
 Hirschmann, M.M. 2000, *Geochem. Geophys. Geosystems*, 1, 1042
 Hodgkin, S.T., & Pye, J.P. 1994, *MNRAS*, 267, 840
 Holman, M., & Murray, N. 2005, *Science*, 307, 1288
 Hsieh, H.H., Jewitt, D., Lacerda, P., Lowry, S.C., & Snodgrass, C. 2010, *MNRAS*, 403, 363
 Jacoby, G.H., Hunter, D.A., & Christian, C.A. 1984, *ApJ Supp.*, 56, 257
 Jäschke, C. & Jäschke, M. 1987, “The Classification of Stars”, Cambridge Univ. Press, Cambridge
 Jenkins et al. 2010, *ApJ*, 724, 1108
 Jessup, K.L., & Spencer, J.R. 2012, *Icarus*, 218, 378
 Jewitt, D. 1996, *Earth, Moon, and Planets*, 72, 185
 Kimura, H., Mann, I., Biesecker, D.A., & Jessberger, E. K. 2002, *Icarus*, 159, 529
 Kotson, M., Rappaport, S., & Levine, A. 2012, in preparation.
 Lamers, H.J.G.L.M., & Cassinelli, J.P. 1999, *Introduction to Stellar Winds*, (Cambridge, UK: Cambridge University Press)
 Lecavelier des Etangs, A. 2007, *A&A*, 461, 1185
 Lecavelier des Etangs, A., et al. 2010, *A&A*, 514, 72
 Léger, A., et al. 2009, *A&A*, 506, 287
 Léger, A., et al. 2011, *Icarus*, 312, 1
 Lemaire, J.F. 2011, *arXiv:1112.3850*
 Linsky, J.L., Yang, H., France, K., Froning, C.S., Green, J.C., Stocke, J.T., & Osterman, S.N. 2010, *ApJ*, 717, 1291
 Madhusudhan, N., Burrows, A., & Currie, T. 2011, *ApJ*, 737, 34
 Marsch, E., Axford, W.I., & McKenzie, J.F. 2003, in *Dynamic Sun*, (Cambridge, UK: Cambridge University Press), editor B.N. Dwivedi, p. 374
 Mikkola, S. 2008, *Multiple Stars Across the H-R Diagram*, ESO Astrophysics Symposia. ISBN 978-3-540-74744-4. (Springer-Verlag: Berlin, Heidelberg), p. 11
 Muirhead, P.S., et al. 2012, *ApJ*, in press, *arXiv:1201.2189*
 Murray-Clay, R., Chiang, E., & Murray, N. 2009, *ApJ*, 693, 23
 Podsiadlowski, Ph., Rappaport, S., Fregeau, J., & Mardling, R. 2010, *arXiv:1007.1418*
 Prsa, A., et al. 2011, *AJ*, 141, 83
 Rauer, H. 2007, in *Trans-Neptunian Objects and Comets*, Saas-Fee Advanced Courses, 35, 165
 Schaefer, L. & Fegley, B., Jr 2009, *ApJ*, 703, L113
 Schaefer, L. Lodders, K., & Fegley, B., Jr 2011, *arXiv:1108.4660*
 Taddeucci, J., Scarlato, P., Capponi, A., et al. 2012, *Geophysical Research Letters*, 39, 2301
 Valencia, D., Sasselov, D.D., & O’Connell, R.J. 2007, *ApJ*, 665, 1413
 van Summeren, J., Conrad, C. P., & Gaidos, E. 2011, *ApJL*, 736, L15
 Vidal-Madjar, A., Désert, J.-M., Lecavelier des Etangs, A., et al. 2003, *Nature*, 422, 143
 Volkov, A.N., et al. 2011, *ApJL*, 729, L24
 Windhorst, R.A., et al. 1991, 380, 362
 Winn, J. N., et al. 2011, *ApJ Lett.*, 737, 18
 Wood, B.E., Müller, H.-R., Zank, G.P., Linsky, J.L., & Redfield, S. 2005, *ApJ*, 628, L143
 Yelle, R.V. 2004, *Icarus*, 167, 30